Electronic Supplementary Material (ESI) for Physical Chemistry Chemical Physics.

Electronic Supplementary Information

Formation of Dimethyl Carbonate via Direct Esterification of CO_2 with Methanol on reduced or stoichiometric CeO_2 (111) and (110) Surfaces

Jian Jiang, Chris M. Marin, Avinash Kumar Both, Chin Li Cheung, Lei Li*, and Xiao Cheng Zeng*

Department of Chemistry, University of Nebraska-Lincoln, Lincoln, NE 68588

To whom correspondence should be addressed:

lil33@sustech.edu.cn; xzeng1@unl.edu

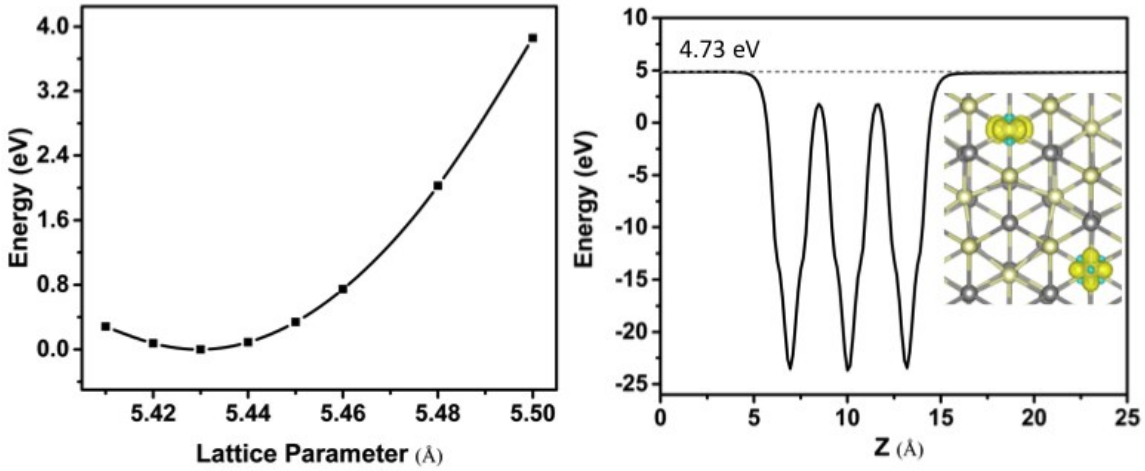

Figure S1. Computed total energy per unit cell of the bulk CeO_2 versus the lattice parameter (left panel). The right panel shows potential distribution along the Z direction for the simulated CeO_2 slab with one oxygen vacancy on the surface. The value 4.73 eV is the computed work function. The inset image shows the spin density of the CeO_2 (111) surface with one oxygen vacancy, suggesting Ce^{3+} is located next-nearest to the oxygen vacancy. The gray and the ivory balls represent oxygen and cerium atoms, respectively.

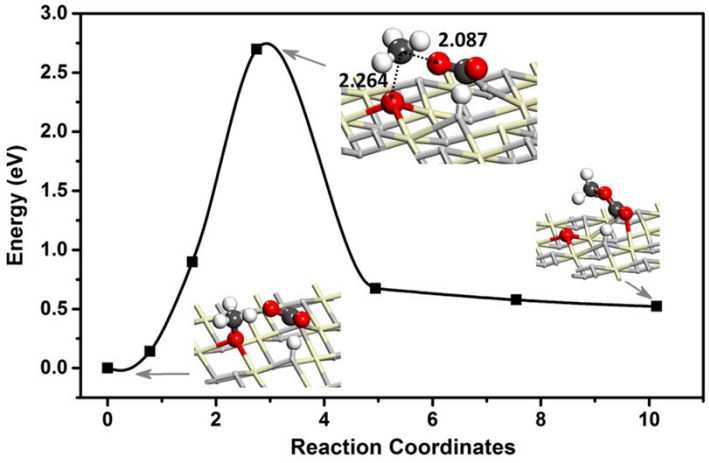

Figure S2. Energy profile computed for the reaction between the methoxy group and the adsorbed CO_2 molecule (in the bent configuration) on the reduced CeO_2 (111). The inset images represent the geometric structures for the reactant, transition and product states, respectively. The bond lengths are labelled in unit Å. The white, black, grey, red and ivory balls represent H, C, O in CeO_2, O in CO_2 and methanol, and Ce atoms, respectively.

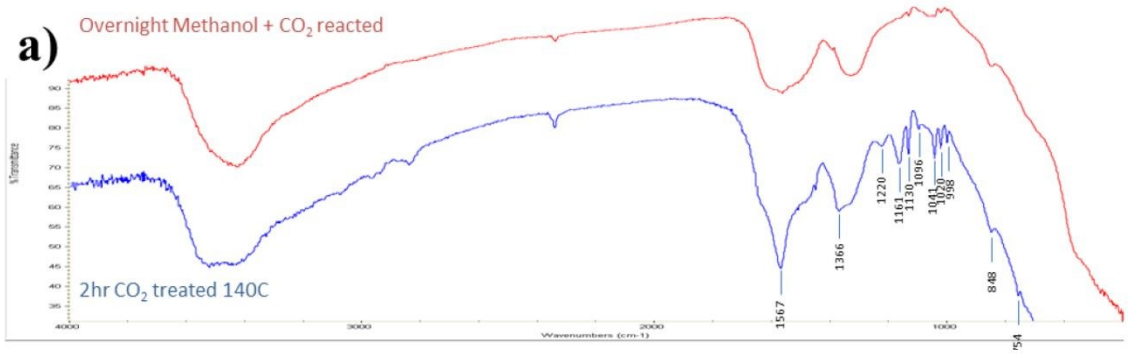

b) CO_2 Peaks Lost or diminished: 1567, 1366, 1161, 1130, 1041, 1020, 998

Figure S3. (a) Measured FTIR transmission spectra of CO_2 on treated ceria after cooling and venting (blue curve) and after a subsequent treatment with methanol (red curve). Note the pronounced peaks from 1567 cm^{-1} to about 1000 cm^{-1} which are removed after reacting with methanol at room temperature. (b) Peak positions (in cm^{-1}) which were found removed by the methanol compared to peak positions published for CO_2 on ceria. [Figure is taken from a PhD thesis[1]]

Table S1. Activation barrier of each elementary reaction for the DMC formation on the CeO_2(111) surface. The symbol '*' represents the active site. The activation energy of the barrierless reaction is set as 0.01 eV and the corresponding reverse reaction is accordingly adjusted. The geometric structure of each state is presented in Figure S4.

	Elementary reactions	Forward reaction barrier (eV)	Reverse reaction barrier (eV)
Stoichiometric active site	**R1.** $CO_2 + * \rightarrow CO^{*}{}_2^{linear}$	**0.01**	**0.27**
	R2. $ME + * \rightarrow ME^*$	**0.01**	**0.77**
	R3. $CO^{*}{}_2^{linear} \rightarrow CO^{*}{}_2^{bent}$	**0.18**	**0.67**
	R4. $CO^{*}{}_2^{linear} + ME^* \rightarrow MMC^* + H^*$	**0.24**	**0.16**
	R5. $CO^{*}{}_2^{bent} + ME^* \rightarrow MMC^* + H^*$	**0.67**	**0.20**
	R6. $MMC^* + ME^* \rightarrow DMC^* + OH^*$	**2.78**	**1.53**
	R7. $DMC^* \rightarrow DMC$	**0.54**	**0.01**
	R8. $H^* + OH^* \rightarrow H_2O$	**0.38**	**0.01**
Reduced active site	**R9.** $CO_2 + *_{vacancy} \rightarrow CO^{*}{}_2^{linear}$	**0.01**	**0.44**
	R10. $ME + *_{vacancy} \rightarrow ME^*$	**0.01**	**1.03**
	R11. $CO^{*}{}_2^{linear} \rightarrow CO^{*}{}_2^{bent}$	**0.09**	**0.77**
	R12. $CO^{*}{}_2^{linear} + ME^* \rightarrow MMC^* + H^*$	**0.01**	**1.38**
	R13. $CO^{*}{}_2^{bent} + ME^* \rightarrow MMC^* + H^*$	**2.71**	**2.21**
	R14. $MMC^* + ME^* \rightarrow DMC^* + H^*$	**1.00**	**0.43**
	R15. $DMC^* \rightarrow DMC$	**0.66**	**0.01**
	R16. $H^* + OH^* \rightarrow H_2O^* + *_{vacancy}$	**1.41**	**0.02**
	R17. $H_2O^* \rightarrow H_2O$	**0.74**	**0.01**

Table S2. Activation barrier of elementary reaction of DMC formation on the CeO_2(110) surface. The symbol '*' represents the active site. The activation energy of the barrierless reaction is set as 0.01 eV and the corresponding reverse reaction is accordingly adjusted. The geometric structure of each state is presented in Figure S5.

	Elementary reactions	Forward reaction barrier (eV)	Reverse reaction barrier (eV)
Stoichiometric active site	**R1.** $CO_2 + * \rightarrow CO^{*\,linear}_{2}$	**0.01**	**0.41**
	R2. $ME + * \rightarrow ME^*$	**0.01**	**1.11**
	R3. $CO^{*\,linear}_{2} \rightarrow CO^{*\,bent}_{2}$	**0.05**	**1.24**
	R4. $CO^{*\,linear}_{2} + ME^* \rightarrow MMC^* + H^*$	**0.29**	**2.19**
	R5. $CO^{*\,bent}_{2} + ME^* \rightarrow MMC^* + H^*$	**1.09**	**1.00**
	R6. $MMC^* + ME^* \rightarrow DMC^* + OH^*$	**3.26**	**2.16**
	R7. $DMC^* \rightarrow DMC$	**0.99**	**0.01**
	R8. $H^* + OH^* \rightarrow H_2O$	**1.14**	**0.01**
Reduced active site	**R9.** $CO_2 + *_{vacancy} \rightarrow CO^{*\,linear}_{2}$	**0.01**	**0.42**
	R10. $CO^{*\,linear}_{2} \rightarrow CO^{*\,bent_2}_{2}$	**0.11**	**1.54**
	R11. $ME + *_{vacancy} \rightarrow ME^*$	**0.01**	**1.32**
	R12. $CO^{*\,bent_2}_{2} \rightarrow CO^{*\,bent^{rotated}}_{2}$	**0.27**	**0.01**
	R13. $CO^{*\,linear}_{2} \rightarrow CO^{*\,bent_1}_{2}$	**0.27**	**1.30**
	R14. $CO^{*\,linear}_{2} + ME^* \rightarrow MMC^* + H^*$	**0.39**	**1.26**
	R15. $CO^{*\,bent_2}_{2} + ME^* \rightarrow MMC^* + H^*$	**0.53**	**0.09**
	R16. $CO^{*\,bent^{rotated}}_{2} + ME^* \rightarrow MMC^* + H^*$	**1.17**	**0.99**
	R17. $CO^{*\,bent^{rotated}}_{2} + ME^* \rightarrow MMC^*_1 + H^*$	**1.09**	**0.86**
	R18. $CO^{*\,bent_1}_{2} + ME^* \rightarrow MMC^* + H^*$	**1.10**	**1.05**
	R19. $MMC^* + ME^* \rightarrow DMC^* + H^*$	**1.39**	**0.47**
	R20. $MMC^*_1 + ME^* \rightarrow DMC^* + H^*$	**1.50**	**0.76**
	R21. $DMC^* \rightarrow DMC$	**0.88**	**0.01**
	R22. $H^* + OH^* \rightarrow H_2O^* + *_{vacancy}$	**1.16**	**0.25**
	R23. $H_2O^* \rightarrow H_2O$	**1.18**	**0.07**

Table S3. Bader charge analysis of pre-absorbed CO_2 (in different configuration) on pristine and reduced CeO_2 (110) and (111) surfaces.

CO_2	Atom Type			Total Charge	Charge Transferred
	C	O	O		
STO_CeO_2 (110)					
Linear	3.48	6.33	6.33	16.14 e	0.14 e
Bent	3.44	6.69	6.70	16.83 e	0.83 e
Ov_CeO_2 (110)					
Linear	3.50	6.33	6.34	16.17 e	0.17 e
$Bent_1$	3.46	6.70	6.71	16.87 e	0.87 e
$Bent_2$	3.44	6.54	6.95	16.93 e	0.93 e
STO_CeO_2 (111)					
Linear	3.46	6.27	6.33	16.07 e	0.07 e
Bent	3.45	6.63	6.62	16.70 e	0.70 e
Ov_CeO_2 (111)					
Linear	3.44	6.20	6.44	16.09 e	0.09 e
Bent	3.46	6.62	6.74	16.81 e	0.81 e

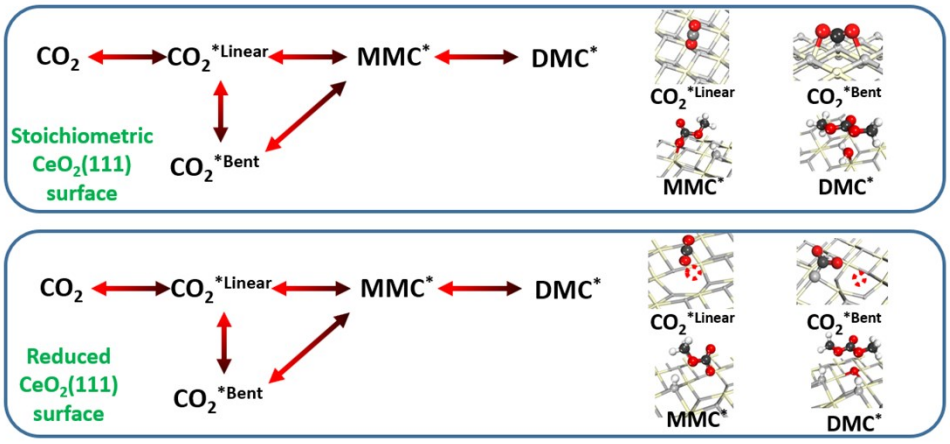

Figure S4. Pathways and intermediates of the DMC formation on the CeO_2 (111) surface.

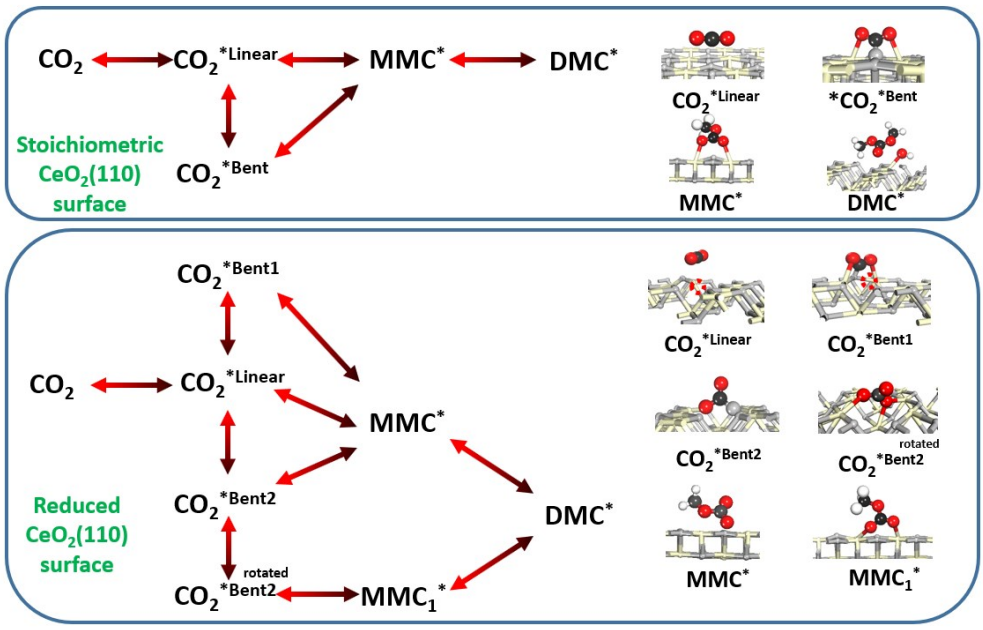

Figure S5. Main pathways and intermediates of the DMC formation on the CeO_2 (110) surface.

Supporting Reference

1. Marin, C. M., *Synthesis and applications of lanthanide sulfides and oxides*. University of Nebraska-Lincoln: 2016.